MEASURING SKID RESISTANCE OF PASSENGER CAR TIRES ON AN INDOOR FACILITY

I. Gusakov, Calspan Corporation

Skid resistance properties of three typical passenger car tires were measured on a wet road surface. A bias ply, a bias belted and a radial ply tire of the G78-14 size series were used in these tests. The tests included straight ahead braking at three speeds and three inclination angles, braking and driving in a turn over a wide range of slip angles, and free rolling cornering and camber. Salient results are presented in the form of plots to demonstrate the capability of the test facility and show the influence of speed, slip angle, inclination angle, and tire construction on the skid characteristics of passenger car tires. A brief description of the test facility and test methods employed in traction testing is included.

Directional stability, control and braking characteristics of vehicles are predominantly influenced by the tires. It is therefore important to define tire performance characteristics through measurements under simulated operational conditions so that vehicle behavior can be predicted and understood. Tire traction properties are most significant in the determination of vehicle safety performance and especially under wet road conditions. This paper deals with these properties by presenting tire test results that were obtained from the Calspan Tire Research Facility (TIRF).

Results which are presented in this paper represent only a fragment of those obtained during tests on the subject tires. A complete description of the test program and the measured results are included in Reference (1). The intent of this presentation is to show trends among bias, bias belted and radial ply tires that are representative of the tested sample and to indicate the form in which data can be quickly and accurately obtained from the TIRF indoor test facility.

Operational features of TIRF are extensively described in Reference (2) and will only be discussed briefly in this paper. Test techniques and operational capabilities of the facility which pertain to traction testing are included in this paper.

TIRF Test Facility

A photograph of TIRF is shown in Figure 1. The primary features of this machine are described in the following discussions.

Tire Positioning System

The tire, wheel system, force sensing balance, wheel disc brake and wheel drive motor are mounted on a moveable head assembly. This assembly provides steer, camber and vertical motions to the tire with respect to the flat roadway beneath the tire. All of these motions are servo controlled and are powered by hydraulic motors. Each system is fully programmable and will accept commands from the TIRF dedicated minicomputer. Vertical motion can be introduced to the tire either as loaded tire radius or vertical load, Fz. The range of the positioning variables and their corresponding maximum rates of change are summarized in Table 1.

Balance System

Two 6 component strain gage balances are available for measuring tire forces and moments. Three orthogonal forces and corresponding moments are measured as reactions in the balance which are transmitted from the tire through a rotating shaft and bearings. Tire torque is measured with a torque transducer which is mounted on a shaft between the tire and drive system. The data reduction system performs necessary transformation to convert forces and moments from the balance axis system to the conventional SAE reference system at the tire roadway as described in Reference (3). The balance system capabilities are summarized in Table 2.

Roadway

The 0.71 m (28 in) wide roadway is comprised of a stainless steel belt covered with a material that simulates the microsurface texture and frictional properties of actual road surfaces. The belt is maintained flat under the tire patch of a loaded tire by support which is provided by a stiff air bearing beneath the belt. The belt is driven by one of the two 1.71 m (67.23 in) diameter drums on which it is installed. Belt speed is servo-controlled hydraulically through electrical programming commands.

The road surface that is most commonly used is "Safety Walk," a material manufactured by the 3M Company. This material provides a friction surface

Figure 1 CALSPAN TIRE RESEARCH FACILITY (TIRF)

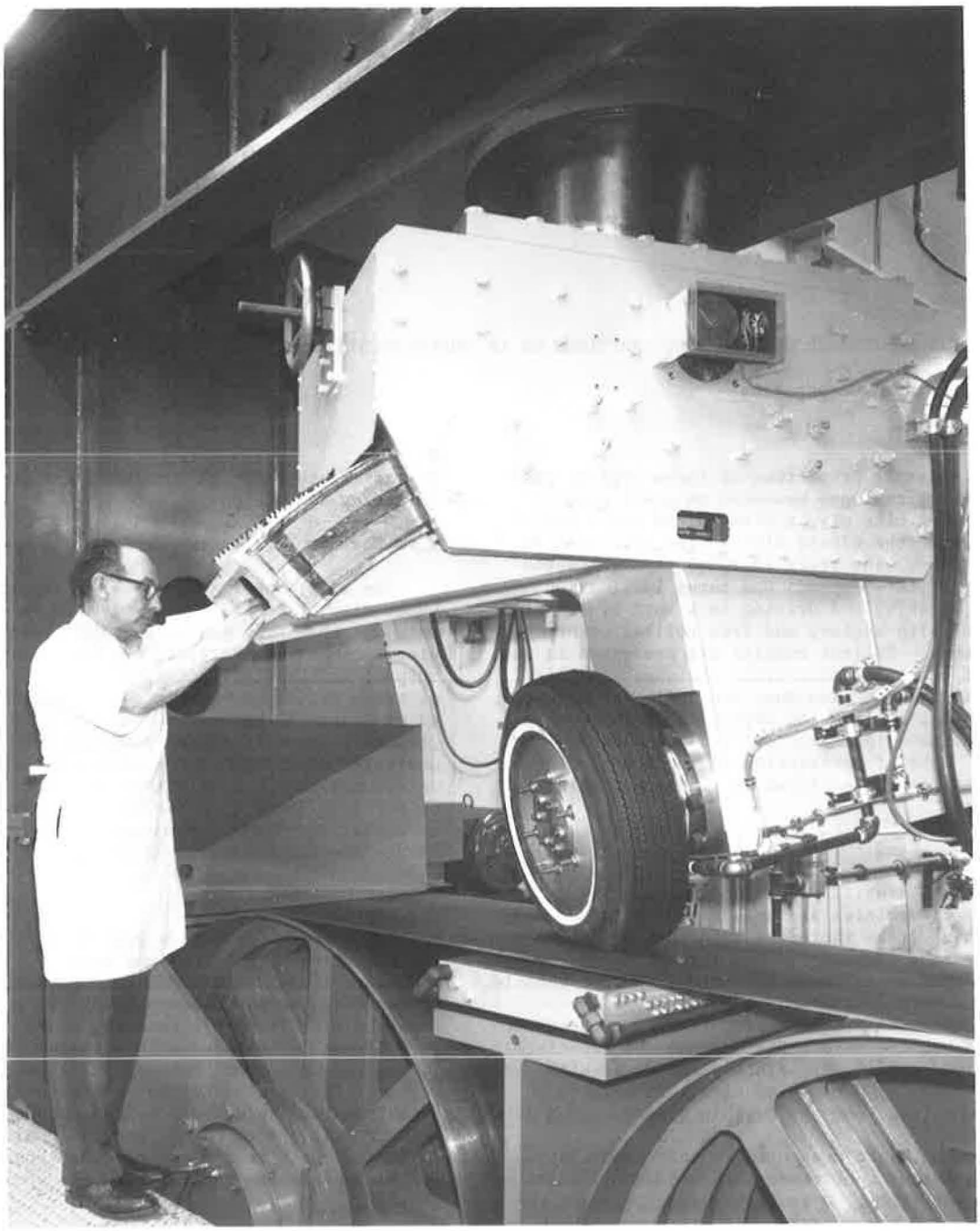

Table 1. TIRF Tire Positioning Capabilities

Positioning Variable	Value
Tire Slip Angle (α)	±30° (±90° with special setup)
Tire Inclination Angle (γ)	±30° (-30° to +54° with special setup)
Tire Slip Angle Rate ($\dot{\alpha}$)	10°/sec
Tire Inclination Angle Rate ($\dot{\gamma}$)	7°/sec
Tire Vertical Positioning Rate ($\dot{z}$)	0.05 m/s (2 in/sec)
Tire Load Rate ($\dot{F}z$) Typical	8900 N/s (2000 lb/sec)
Road Speed (V)	0-322 km/h (0-200 mph)

Table 2. Balance System Capabilities

Component	Passenger Car Tire Balance	Truck Tire Balance
Vertical Load (Fz)	17793 N (4000 lb)	53379 N (12000 lb)
Tractive Force (Fx)	±17793 N (±4000 lb)	±35586 N (±8000 lb)
Lateral Force (Fy)	±17793 N (±4000 lb)	±35586 N (±8000 lb)
Aligning Torque (Mz)	±678 Nm (±500 ft lb)	±1356 Nm (±1000 ft lb)
Overturning Moment (Mx)	±1356 Nm (±1000 ft lb)	±2712 Nm (±2000 ft lb)
Rolling Resistance Moment (My)	±271 Nm (±200 ft lb)	±542 Nm (± 400 ft lb)
Wheel Torque (T)	±6780 Nm (±5000 ft lb)	±6780 Nm (±5000 ft lb)

with a skid number of approximately 60 as received when measured with an ASTM E-501 Standard Pavement Traction Tire at 64 km/h (40 mph) and 0.5 mm (0.020 in) water depth. Friction of this material is easily controlled to any desired level of skid number between 25 and 60 by stoning. The test surfaces most typically used have skid numbers of 30 and 50.

A unique feature of TIRF is that tests can be conducted under wet road surface conditions. A two dimensional water nozzle deposits a layer of water tangential to the road surface with a flow rate that corresponds to the linear speed of the belt. Water flow rate is controlled by the upstream nozzle pressure and water depth is regulated from 0 to 10 mm (0.4 in) by adjusting the throat of the nozzle.

Figure 2 shows a tire undergoing wet testing on TIRF.

Figure 2 TIRE UNDERGOING WET TESTING ON TIRF

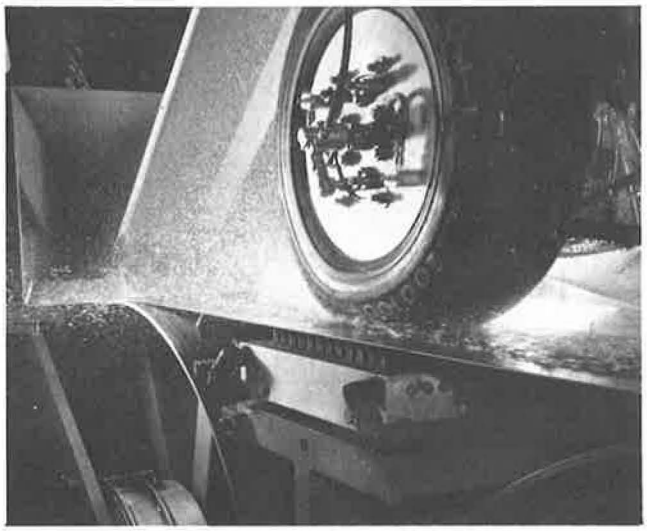

Wheel Drive System

A hydraulic drive system, which is independent of the roadway drive, is connected to the tire through a gearbox. The gearbox permits selection of the optimum torque-speed characteristics for traction testing. Two methods of obtaining tire traction characteristics are available with the hydrostatic drive system and are depicted in the simplified block diagram of Figure 3. An electrical input command is programmed into the system which produces either controlled tire speed or torque response, depending upon which mode of operation is chosen. The input command is compared to the corresponding feedback signal from either wheel speed or torque and the error is amplified. This amplified error signal is applied to the variable displacement pump servosystem, which produces the necessary change in the hydraulic motor speed or torque characteristics to maintain system control. A torque transducer, which is coupled between the output of the gearbox and the tire, generates the torque feedback signal. This signal is used for stability compensation of the servosystem in the speed control mode and for direct coupled feedback when wheel torque control is employed. Wheel speed is sensed by a d.c. tachometer for feedback purposes in the control of the system.

Speed control is used most often in traction performance testing of tires. The system input command originates in the TIRF computer and represents a longitudinal slip ratio setpoint in this mode of operation. Control of the tire is maintained throughout the entire traction range of slip from -1 to +1 or full tire lockup to full driving. Since slip ratio has two values at a given tractive force around the peak region, slip ratio, or wheel speed control, is the only practical scheme which can result in measurements over the entire traction field with stability. The multivalued nature of slip ratio as a function of traction is exhibited in the plots of Figures 5 through 8 of this paper.

Torque feedback control is useful in conducting tests in which the effect of small perturbations of slip ratio, below peak traction, are investigated. Measurement of tire rolling resistance under traction are very successful when applying this control technique.

The hydraulic motor has limited torque capabilities and consequently it is often necessary to use an auxilliary traction control system. A closed loop servosystem with a hydraulically activated caliper disc brake system is employed for this purpose. A simplified block diagram of this system is shown in Figure 4. A shortcoming of this system is that only braking traction tests can be performed since the brake can only absorb power.

Operation of this system is similar to that of the hydraulic motor speed control. An electrical input command produces a wheel speed by modulating the disc brake as required to maintain control. This input is usually a linear ramp that produces a constant deceleration of the wheel and thus induces minimum dynamic excitation of the test tire. The programmed input setpoint is combined with the speed feedback signal and the resulting error is amplified. The amplified error signal actuates the brake through the servosystem as necessary to maintain tire speed control. Speed feedback is gener-

Figure 3 SIMPLIFIED BLOCK DIAGRAM OF THE WHEEL TRACTION CONTROL SYSTEM WITH THE HYDRAULIC MOTOR

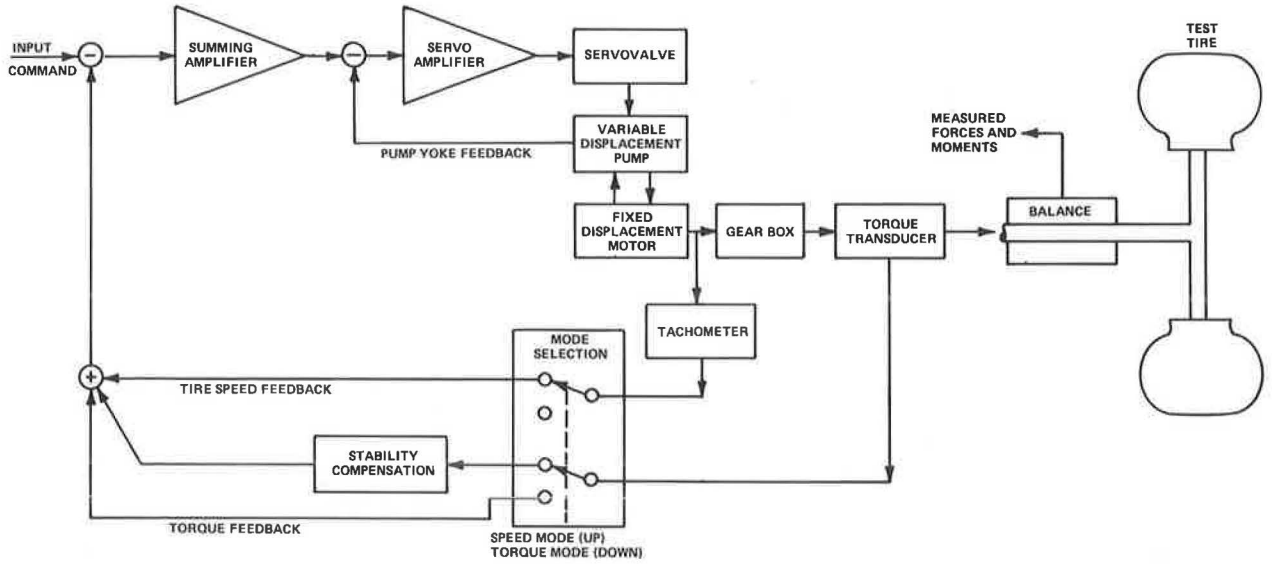

Figure 4 SIMPLIFIED BLOCK DIAGRAM OF THE WHEEL TRACTION CONTROL SYSTEM WITH THE DISC BRAKE

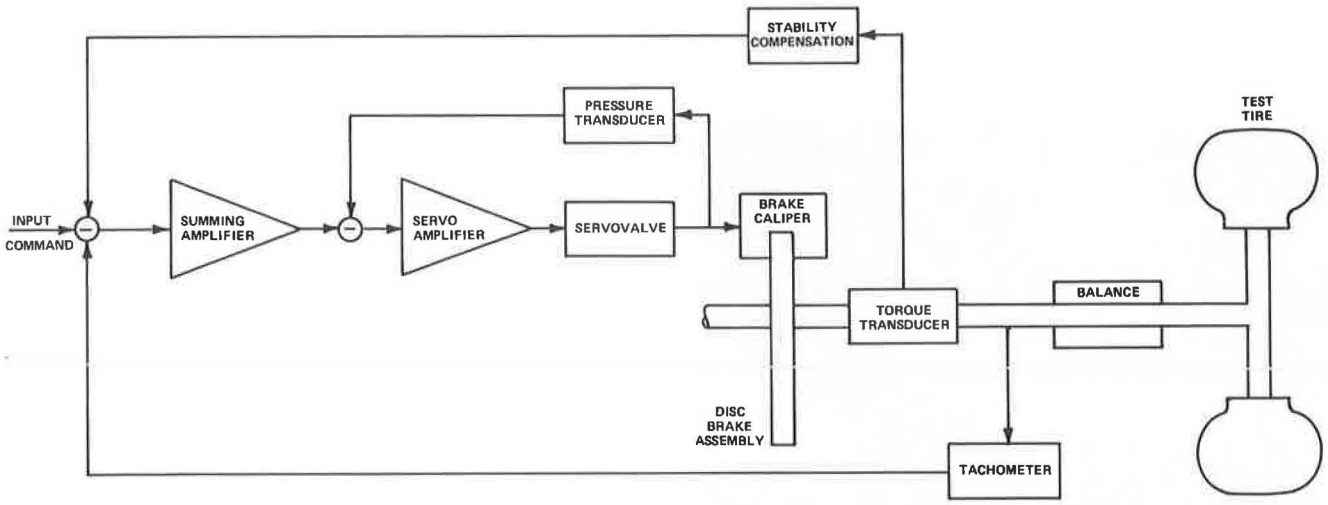

ated by a noncontacting digital tachometer. This tachometer signal is also used to measure slip ratio during testing and is recorded by the TIRF minicomputer.

Maximum operating capabilities of the TIRF hydraulic motor driven traction control system are summarized in Table 3.

Table 3. Operating Capabilities of the TIRF Hydraulic Motor Driven Traction Control System

Gearbox Range	Wheel Speed RPM	Torque
1	694	3670 Nm (2707 ft lb)
2	1800	1417 Nm (1045 ft lb)
3	2400	1063 Nm (784 ft lb)

Disc brake operational limitations are those associated with the roadway drive system and the wheel torque transducer capacity. The roadway can be presently driven at speeds up to 282 km/h (175 mph). The drum system inertia reflected to the surface of the roadway in contact with the tire is equivalent to a linear weight of 12000 N (2700 lb). Four speed ranges are available in the roadway system and these are summarized with corresponding theoretical tractive force capabilities in Table 4.

Table 4. Operating Capabilities of the TIRF Roadway Drive System

Gear Range	Gear Ratio	Maximum Speed	Maximum Tractive Force
1	7.47	77 km/h (48 mph)	12455 N (2800 lb)
2	4.83	140 km/h (87 mph)	8007 N (1800 lb)
3	3.13	185 km/h (115 mph)	5200 N (1168 lb)
4	1.99	290 km/h (180 mph)	3303 N (742 lb)

The maximum capacity of the torque transducer is 6780 Nm (5000 ft lb), which, on occasion, can be exceeded by 20% providing that no torque measurements are required and the dynamic excitation of the tire is at a low level.

Test Program

Simulated wet road tests were conducted on three tires: a bias, bias belted and a radial ply of the G78-14 size series. These tires are listed in Table 5 along with the test schedule that summarizes the range of variables used in the tests. The information contained in this table is self-explanatory. A water depth of 0.5 mm (0.020 in) was used in all of these tests. Additional tests were conducted on these tires and all results are presented in Reference (1). Only traction test results are discussed in this paper.

Each of the three tires was tested under identical conditions as specified in Table 5. The influence of slip angle on tire behavior over the full range of driving and braking traction was investigated. The effects of speed and inclination angle on braking traction were also measured.

Tests were conducted under computer control employing the continuous sampling technique of data acquisition. With this technique it is possible to sample at rates up to 100 samples per second and up to 660 samples while any number of test variables are changing. Data filters with low pass characteristics were used to reduce scatter produced by tire nonuniformity and vibrations. The result of the use of filters is a steady state representation of the characteristics. The choice of filters is dependent upon the signal frequencies which are present in the results. Rates of change of test variables must be slow in comparison to the filter bandwidth so that attenuation of desirable information does not occur. It has been observed that if a filter with a low pass band is used and the time that a tire traction response passes though the peak is short in comparison to the filter time constant, attenuation and delay of the peak information will result. This often leads to erroneous conclusions about the effect of rate of traction application on the traction behavior of tires as pointed out in Reference (4). A combination of test variable sweep rates and filter pass bands was chosen that produced faithful reproduction of the tire characteristics. Low pass, single pole, data filters with a 1/4 Hz corner frequency and four-pole cascade filters with a 10 Hz corner frequency were used in these tests. All six balance signals, as well as wheel and road speed information, where conditioned with these filters.

Table 5. Test Schedule

Run No.	Tire No.	Road Speed v	Slip Angle α	Incl. Angle γ	Long'l. Slip
205		32 km/h (20 mph)	B	0	
206	14	32 km/h (20 mph)	A	0	-1→ +1
207		32 km/h (20 mph)	C	0	
208		A	0	A	0→ -1
209		32 km/h (20 mph)	A	0	
210	33	32 km/h (20 mph)	B	0	-1→ +1
211		32 km/h (20 mph)	C	0	
212		A	0	A	0→ -1
213		32 km/h (20 mph)	A	0	
214	156	32 km/h (20 mph)	B	0	-1→ +1
215		32 km/h (20 mph)	C	0	
216		A	0	A	0→ -1

α (A) 0, ±4, ±16 deg

α (B) ±1, ±8 deg

α (C) ±2, ±24 deg

γ (A) 3, 6 deg

v (A) 32, 64 and 97 km/h (20, 40, and 60 mph)

F_z Test Load 4893 N (1100 lb)

Inflation Pressure 165 k Pa (24 psi)
Road Skid Number 33

Tire No 14 G78-14 Bias Belted Dunlop Gold Seal "78" Sport
Tire No 33 GR78-14 Radial Ply Goodyear Steelgard Radial
Tire No 156 G78-14 Bias Ply B.F.Goodrich Classic HT

Tire Traction Test Results

Measured wet traction characteristics of the bias belted, radial and bias tires are presented as plots of reduced data. Variations of lateral force, Fy, tractive force, Fx, and aligning torque, Mz, with slip ratio, SR, and slip angle, α, are summarized in the plots of Figures 5 through 20.

Figure 5 shows the effects of slip angle over the range from -24 to 24 degrees on tractive force. Slip ratio is defined by the relationship:

$$SR = (WR_L/V \cos \alpha)-1,$$

where W is the wheel spin velocity, R_L is the loaded radius of the tire, and V is the road speed. This definition is employed throughout all of the data presentation in this paper. Data represented by this plot show the general trend of slip angle variations over the entire test range for the bias belted tire. Data points were sampled close together and displayed a continuous pattern when plotted. Values of tractive force under full wheel lockup and full driving (SR = ±1) conditions did not vary with slip angle. The peak values did change however and at large values of α, above 16°, it became difficult to define a peak in the tractive force characteristics. Also, as slip angle increased, the slip ratio at which peak tractive force occurred increased. For example, the peak tractive force occurred at a slip ratio of 0.2 at 4° slip angle and at 0.1 slip ratio when the slip angle was zero. The value of the peak tractive force also decreased with increasing slip angle. These general trends also apply to the radial and bias tires.

Figure 5. PLOT OF TRACTIVE FORCE (F_x) VERSUS SLIP RATIO (SR) FOR THE BIAS BELTED TIRE

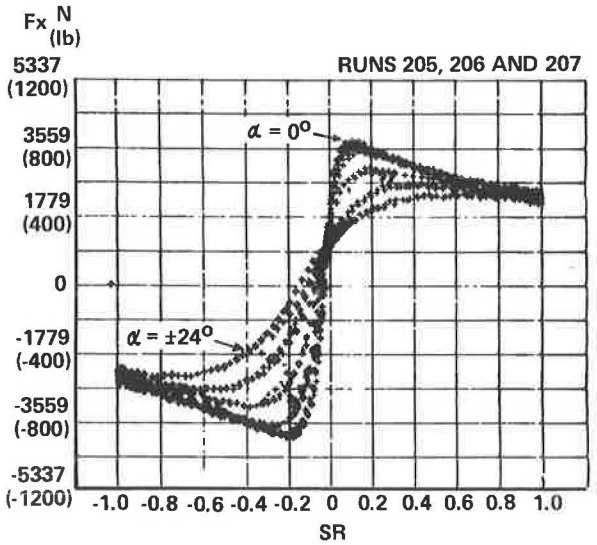

TEST CONDITIONS:

WATER DEPTH	0.5 mm (0.020 in)
LOAD	6228 N (1400 lb)
INFLATION PRESSURE	165 kPa (24 psi)
SPEED	32 km/h (20 mph)
SLIP ANGLE (α)	0° TO ±24°
INCLINATION ANGLE (γ)	0°

Figure 6. PLOT OF TRACTIVE FORCE (Fx) VERSUS SLIP RATIO (SR) FOR THE BIAS BELTED TIRE

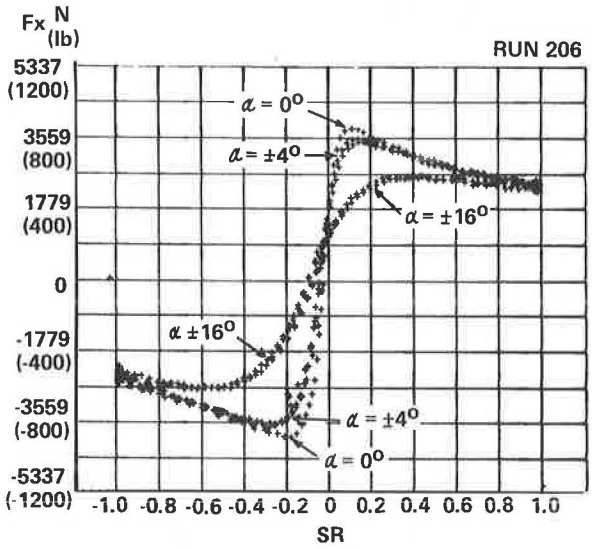

TEST CONDITIONS:

WATER DEPTH	0.5 mm (0.020 in)
LOAD	6228 N (1400 lb)
INFLATION PRESSURE	165 kPa (24 psi)
SPEED	32 km/h (20 mph)
SLIP ANGLE (α)	0°, ±4° AND ±16°
INCLINATION ANGLE (γ)	0°

Figure 7. PLOT OF TRACTIVE FORCE (Fx) VERSUS SLIP RATIO (SR) FOR THE RADIAL TIRE

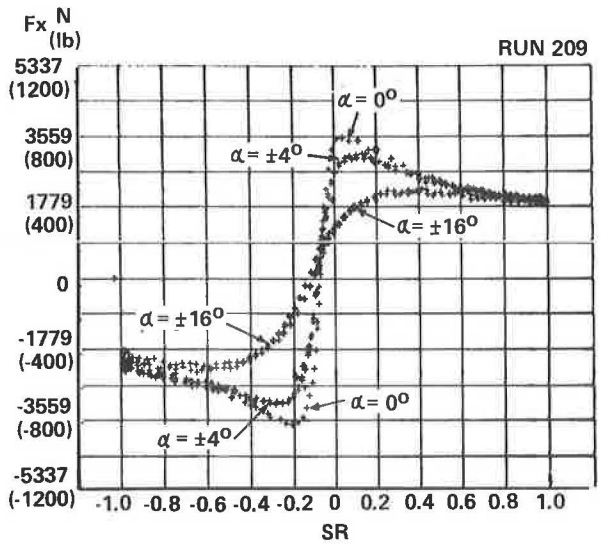

TEST CONDITIONS:

WATER DEPTH	0.5 mm (0.020 in)
LOAD	6228 N (1400 lb)
INFLATION PRESSURE	165 kPa (24 psi)
SPEED	32 km/h (20 mph)
SLIP ANGLE (α)	0°, ±4° AND ±16°
INCLINATION ANGLE (γ)	0°

Figure 8. PLOT OF TRACTIVE FORCE (Fx) VERSUS SLIP RATIO (SR) FOR THE BIAS TIRE

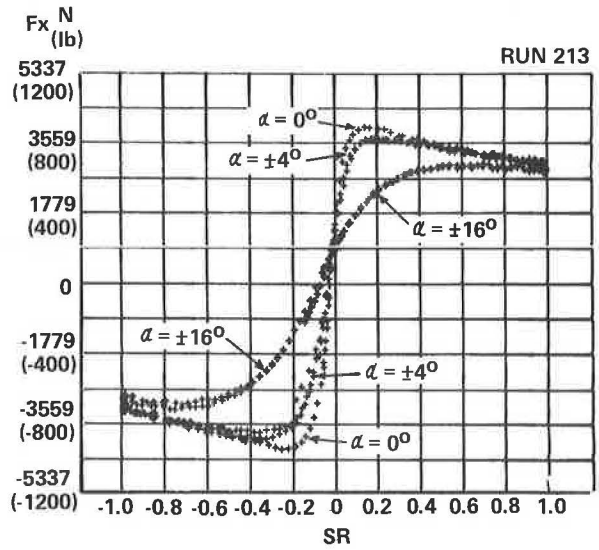

TEST CONDITIONS:

WATER DEPTH	0.5 mm (0.020 in)
LOAD	6228 N (1400 lb)
INFLATION PRESSURE	165 kPa (24 psi)
SPEED	32 km/h (20 mph)
SLIP ANGLE (α)	0°, ±4° AND ±16°
INCLINATION ANGLE (γ)	0°

Figure 9 PLOT OF LATERAL FORCE (Fy) VERSUS SLIP RATIO (SR) FOR THE BIAS BELTED TIRE

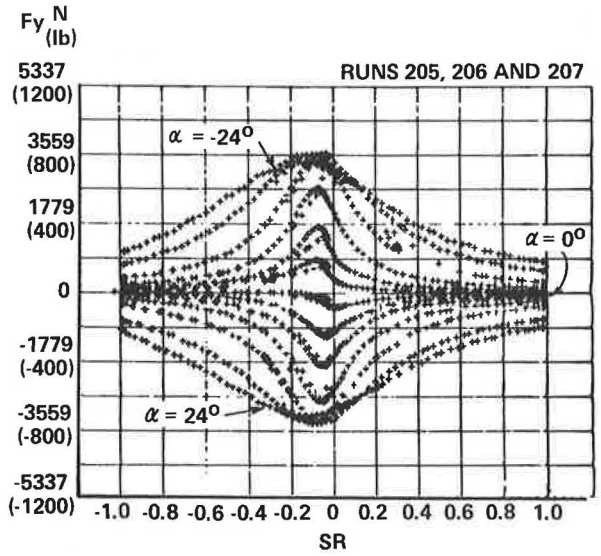

TEST CONDITIONS:

WATER DEPTH	0.5 mm (0.020 in)
LOAD	6228 N (1400 lb)
INFLATION PRESSURE	165 kPa (24 psi)
SPEED	32 km/h (20 mph)
SLIP ANGLE (α)	0° TO ±24°
INCLINATION ANGLE (γ)	0°

Figure 10. PLOT OF LATERAL FORCE (Fy) VERSUS SLIP RATIO (SR) FOR THE BIAS BELTED TIRE

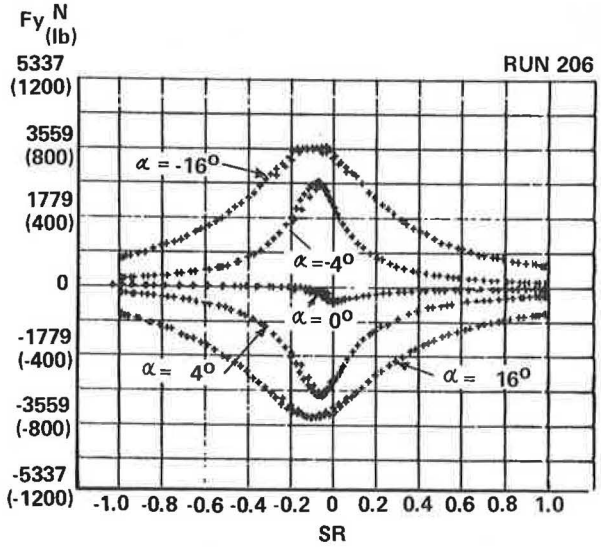

TEST CONDITIONS:

WATER DEPTH	0.5 mm (0.020 in)
LOAD	6228 N (1400 lb)
INFLATION PRESSURE	165 kPa (24 psi)
SPEED	32 km/h (20 mph)
SLIP ANGLE (α)	0°, ±4° AND ±16°
INCLINATION ANGLE (γ)	0°

Figure 11. PLOT OF LATERAL FORCE (Fy) VERSUS SLIP RATIO (SR) FOR THE RADIAL TIRE

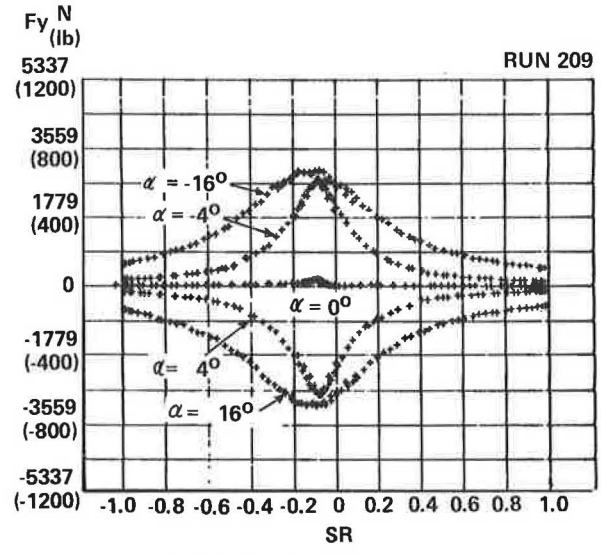

TEST CONDITIONS:

WATER DEPTH	0.5 mm (0.020 in)
LOAD	6228 N (1400 lb)
INFLATION PRESSURE	165 kPa (24 psi)
SPEED	32 km/h (20 mph)
SLIP ANGLE (α)	0°, ±4° AND ±16°
INCLINATION ANGLE (γ)	0°

Figure 12. PLOT OF LATERAL FORCE (Fy) VERSUS SLIP RATIO (SR) FOR THE BIAS TIRE

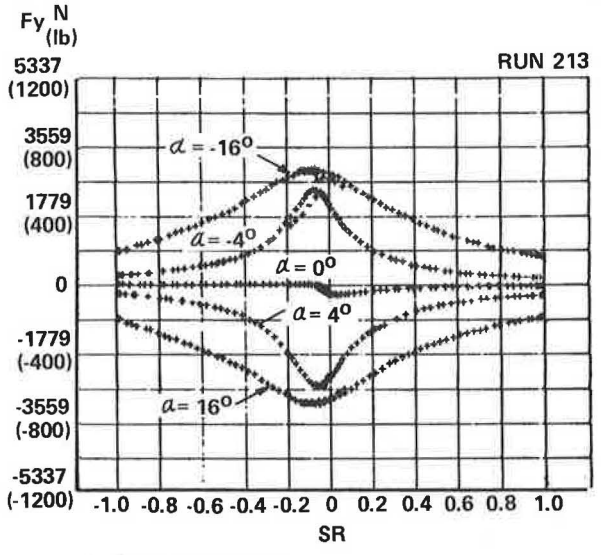

TEST CONDITIONS:

WATER DEPTH	0.5 mm (0.020 in)
LOAD	6228 N (1400 lb)
INFLATION PRESSURE	165 kPa (24 psi)
SPEED	32 km/h (20 mph)
SLIP ANGLE (α)	0°, ±4° AND ±16°
INCLINATION ANGLE (γ)	0°

Figure 13. PLOT OF LATERAL FORCE (F_y) VERSUS TRACTIVE FORCE (F_x) FOR THE BIAS BELTED TIRE

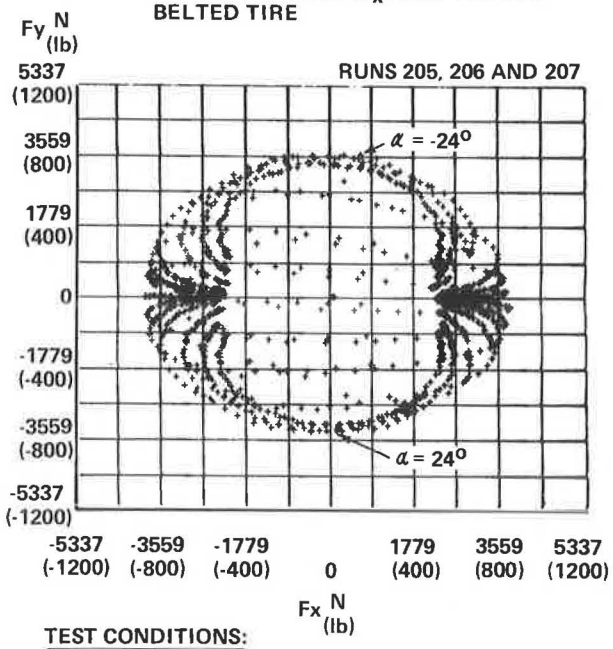

TEST CONDITIONS:

WATER DEPTH	0.5 mm (0.020 in)
LOAD	6228 N (1400 lb)
INFLATION PRESSURE	165 kPa (24 psi)
SPEED	32 km/h (20 mph)
SLIP ANGLE (α)	0° TO ±24°
INCLINATION ANGLE (γ)	0°

Figure 14. PLOT OF LATERAL FORCE (Fy) VERSUS TRACTIVE FORCE (Fx) FOR THE BIAS BELTED TIRE

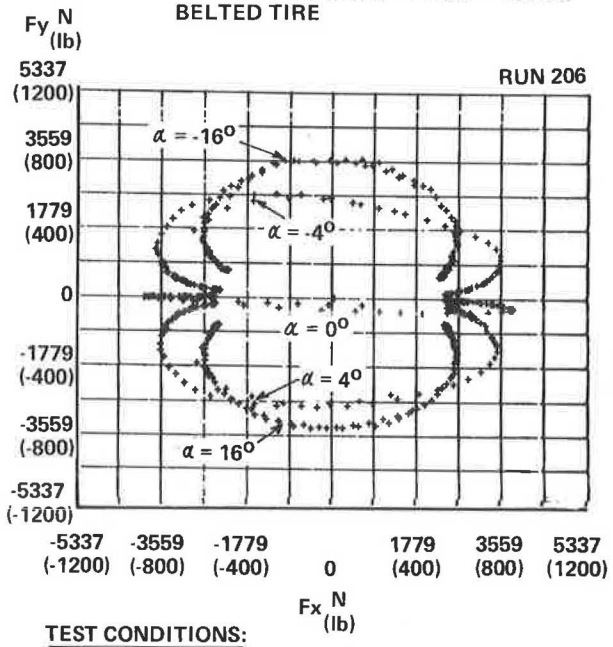

TEST CONDITIONS:

WATER DEPTH	0.5 mm (0.020 in)
LOAD	6228 N (1400 lb)
INFLATION PRESSURE	165 kPa (24 psi)
SPEED	32 km/h (20 mph)
SLIP ANGLE (α)	0°, ±4° AND ±16°
INCLINATION ANGLE (γ)	0°

Figure 15. PLOT OF LATERAL FORCE (Fy) VERSUS TRACTIVE FORCE (Fx) FOR THE RADIAL TIRE

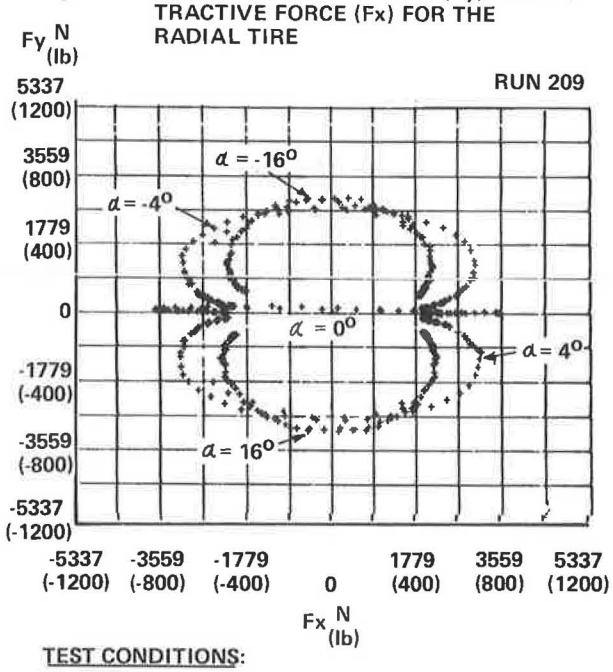

TEST CONDITIONS:

WATER DEPTH	0.5 mm (0.020 in)
LOAD	6228 N (1400 lb)
INFLATION PRESSURE	165 kPa (24 psi)
SPEED	32 km/h (20 mph)
SLIP ANGLE (α)	0°, ±4° AND ±16°
INCLINATION ANGLE (γ)	0°

Figure 16. PLOT OF LATERAL FORCE (Fy) VERSUS TRACTIVE FORCE (Fx) FOR THE BIAS TIRE

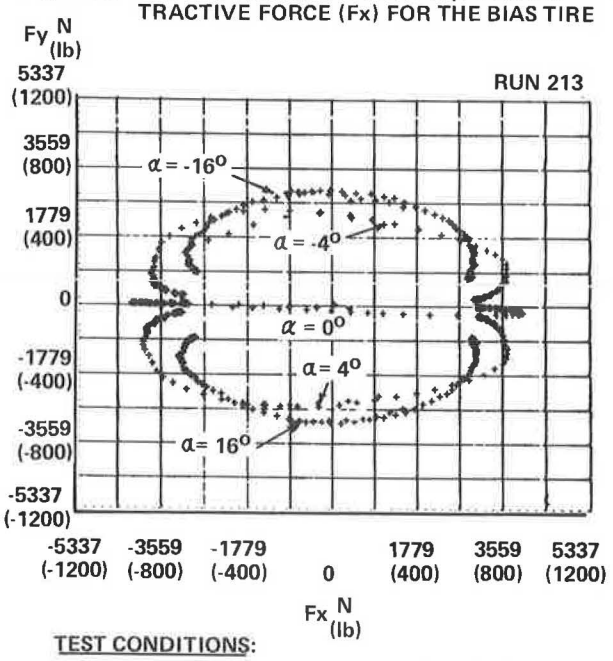

TEST CONDITIONS:

WATER DEPTH	0.5 mm (0.020 in)
LOAD	6228 N (1400 lb)
INFLATION PRESSURE	165 kPa (24 psi)
SPEED	32 km/h (20 mph)
SLIP ANGLE (α)	0°, ± 4° AND ± 16°
INCLINATION ANGLE (γ)	0°

Figure 17. PLOT OF ALIGNING TORQUE (Mz) VERSUS TRACTIVE FORCE (Fx) FOR THE BIAS BELTED TIRE

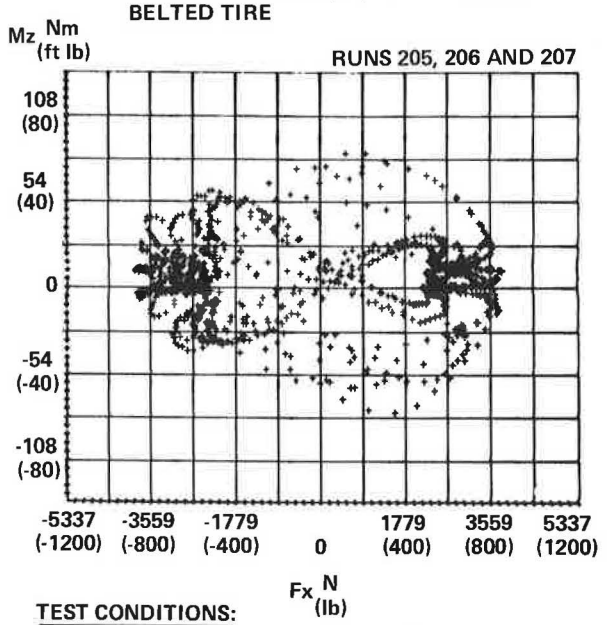

TEST CONDITIONS:

WATER DEPTH	0.5 mm (0.020 in)
LOAD	6228 N (1400 lb)
INFLATION PRESSURE	165 kPa (24 psi)
SPEED	32 km/h (20 mph)
SLIP ANGLE (α)	0^o TO $\pm 24^o$
INCLINATION ANGLE (γ)	0^o

Figure 18. PLOT OF ALIGNING TORQUE (Mz) VERSUS TRACTIVE FORCE (Fx) FOR THE BIAS BELTED TIRE

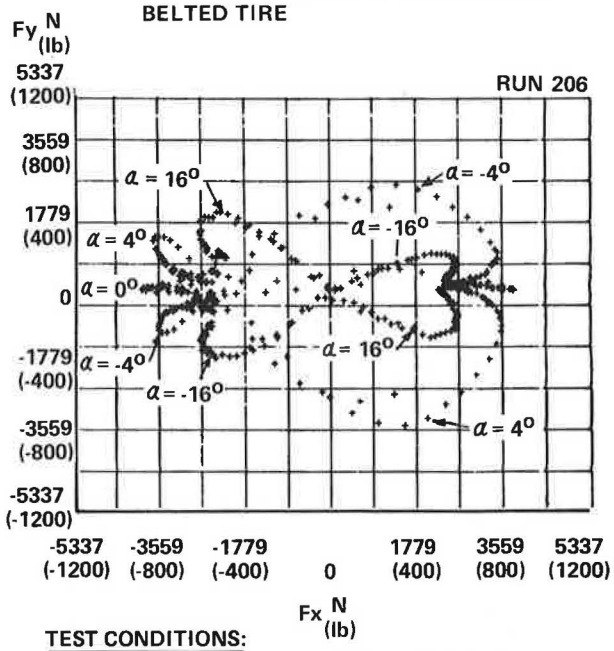

TEST CONDITIONS:

WATER DEPTH	0.5 mm (0.020 in)
LOAD	6228 N (1400 lb)
INFLATION PRESSURE	165 kPa (24 psi)
SPEED	32 km/h (20 mph)
SLIP ANGLE (α)	0^o, $\pm 4^o$ AND $\pm 16^o$
INCLINATION ANGLE (γ)	0^o

Figure 19. PLOT OF ALIGNING TORQUE (Mz) VERSUS TRACTIVE FORCE (Fx) FOR THE RADIAL TIRE

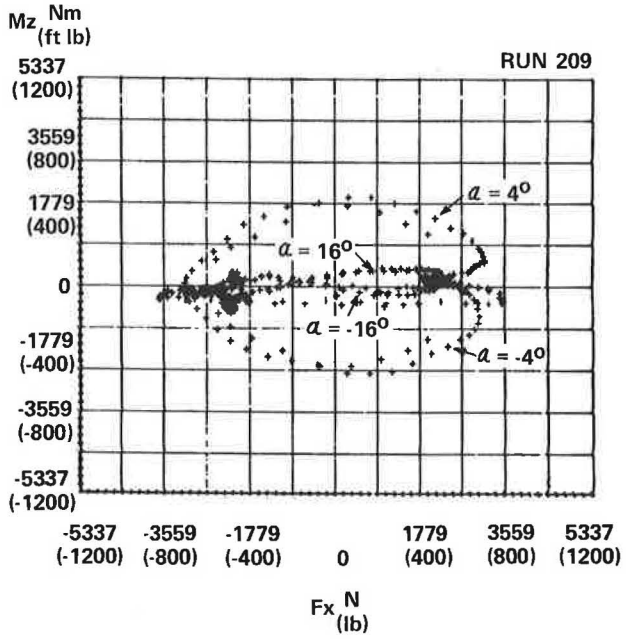

TEST CONDITIONS:

WATER DEPTH	0.5 mm (0.020 in)
LOAD	6228 N (1400 lb)
INFLATION PRESSURE	165 kPa (24 psi)
SPEED	32 km/h (20 mph)
SLIP ANGLE (α)	0^o, $\pm 4^o$ AND $\pm 16^o$
INCLINATION ANGLE (γ)	0^o

Figure 20. PLOT OF ALIGNING TORQUE (Mz) VERSUS TRACTIVE FORCE (Fx) FOR THE BIAS TIRE

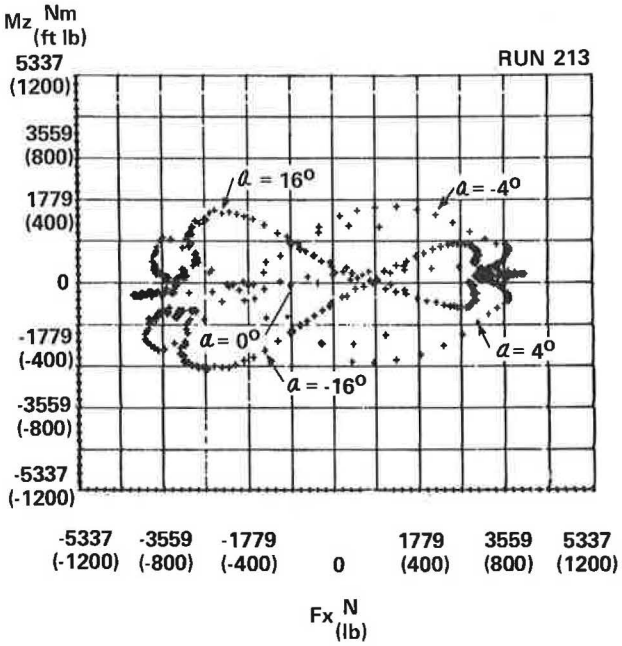

TEST CONDITIONS:

WATER DEPTH	0.5 mm (0.020 in)
LOAD	6228 N (1400 lb)
INFLATION PRESSURE	165 kPa (24 psi)
SPEED	32 km/h (20 mph)
SLIP ANGLE (α)	0^o, $\pm 4^o$ AND $\pm 16^o$
INCLINATION ANGLE (γ)	0^o

Figure 21. PLOT OF TRACTIVE FORCE (Fx) VERSUS SLIP RATIO (SR) AS A FUNCTION OF SPEED FOR THE BIAS BELTED TIRE

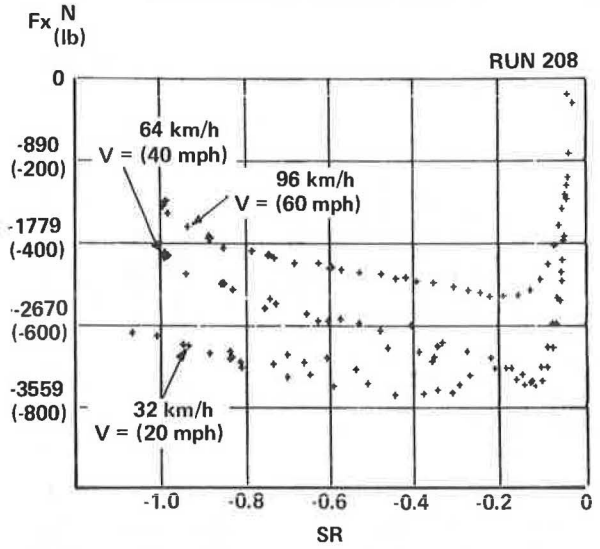

TEST CONDITIONS:

WATER DEPTH	0.5 mm (0.020 in)
LOAD	6228 N (1400 lb)
INFLATION PRESSURE	165 kPa (24 psi)
SPEED	32, 64 AND 96 km/h (20, 40 AND 60 mph)
SLIP ANGLE (α)	0°
INCLINATION ANGLE (γ)	3°

Figure 22. PLOT OF TRACTIVE FORCE (Fx) VERSUS SLIP RATIO (SR) AS A FUNCTION OF SPEED FOR THE RADIAL TIRE

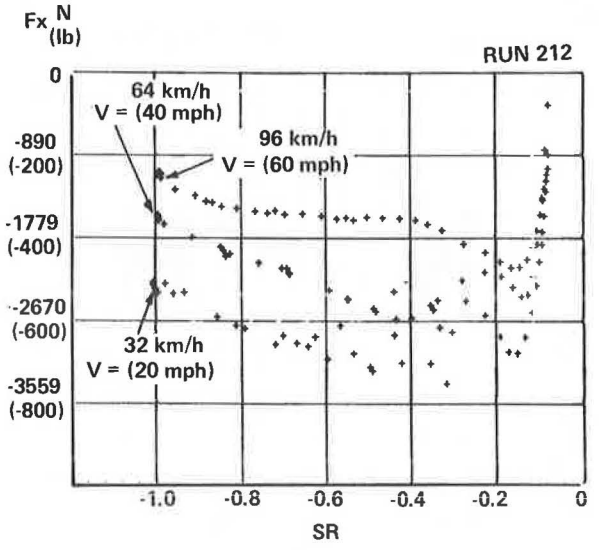

TEST CONDITIONS:

WATER DEPTH	0.5 mm (0.020 in)
LOAD	6228 N (1400 lb)
INFLATION PRESSURE	165 kPa (24 psi)
SPEED	32, 64 AND 96 km/h (20, 40 AND 60 mph)
SLIP ANGLE (α)	0°
INCLINATION ANGLE (γ)	3°

Figure 23. PLOT OF TRACTIVE FORCE (Fx) VERSUS SLIP RATIO (SR) AS A FUNCTION OF SPEED FOR THE BIAS TIRE

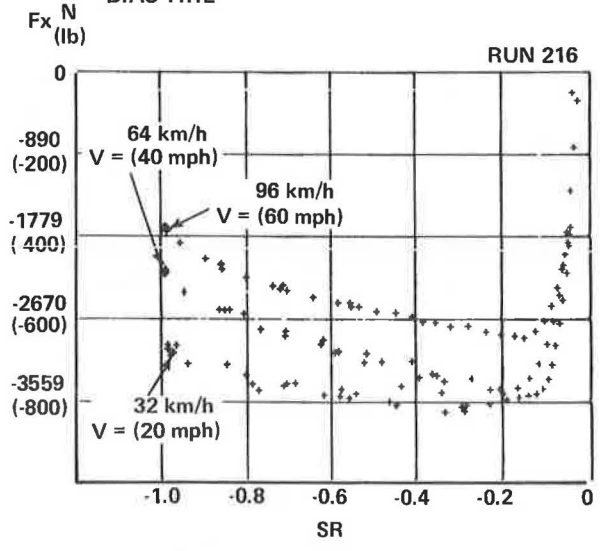

TEST CONDITIONS:

WATER DEPTH	0.5 mm (0.020 in)
LOAD	6228 N (1400 lb)
INFLATION PRESSURE	165 kPa (24 psi)
SPEED	32, 64 AND 96 km/h (20, 40 AND 60 mph)
SLIP ANGLE (α)	0°
INCLINATION ANGLE (γ)	3°

Figure 24. PLOT OF TRACTIVE FORCE (Fx) VERSUS SLIP RATIO (SR) AS A FUNCTION OF SPEED FOR THE BIAS BELTED TIRE

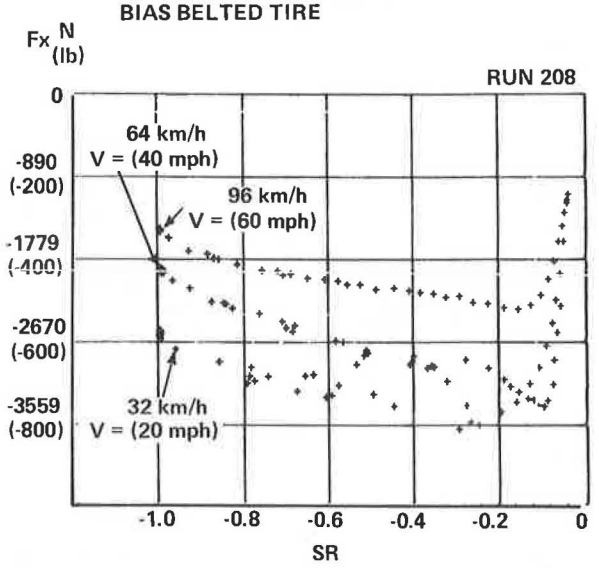

TEST CONDITIONS:

WATER DEPTH	0.5 mm (0.020 in)
LOAD	6228 N (1400 lb)
INFLATION PRESSURE	165 kPa (24 psi)
SPEED	32, 64 AND 96 km/h (20, 40 AND 60 mph)
SLIP ANGLE (α)	0°
INCLINATION ANGLE (γ)	6°

Figure 25. PLOT OF TRACTIVE FORCE (Fx) VERSUS SLIP RATIO (SR) AS A FUNCTION OF SPEED FOR THE RADIAL TIRE

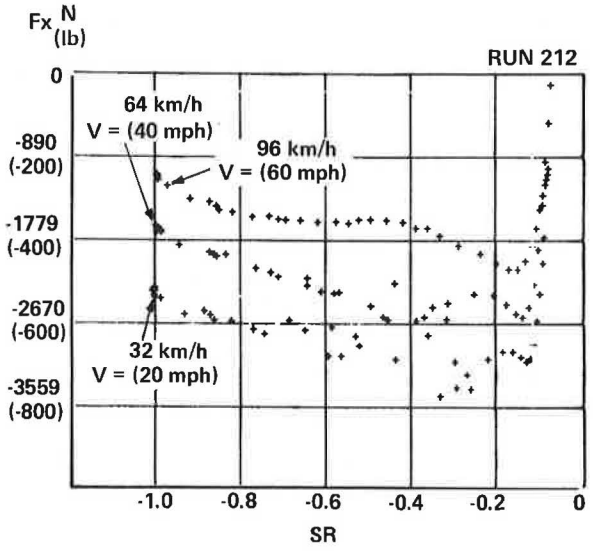

TEST CONDITIONS:

WATER DEPTH	0.5 mm (0.020 in)
LOAD	6228 N (1400 lb)
INFLATION PRESSURE	165 kPa (24 psi)
SPEED	32, 64 AND 96 km/h (20, 40 AND 60 mph)
SLIP ANGLE (α)	0°
INCLINATION ANGLE (γ)	6°

Figure 26. PLOT OF TRACTIVE FORCE (Fx) VERSUS SLIP RATIO (SR) AS A FUNCTION OF SPEED FOR THE BIAS TIRE

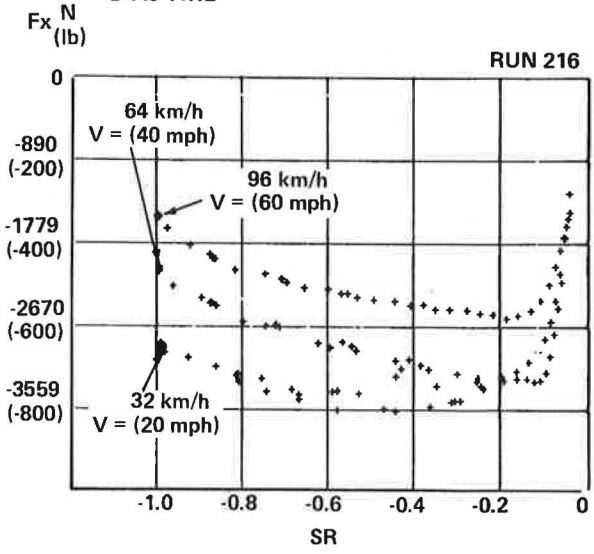

TEST CONDITIONS:

WATER DEPTH	0.5 mm (0.020 in)
LOAD	6228 N (1400 lb)
INFLATION PRESSURE	165 kPa (24 psi)
SPEED	32, 64 AND 96 km/h (20, 40 AND 60 mph)
SLIP ANGLE (α)	0°
INCLINATION ANGLE (γ)	6°

Figures 6, 7 and 8 show selected plots of Fx as a function of α and SR for the bias belted, radial and bias tires respectively. Slip angles were 0, ±4 and ±16 degrees in these plots. These plots indicate that the bias belted tire had measurably better traction than the radial and bias tire. In fact, the bias tire also exhibited better traction behavior than the radial tire over this slip angle range.

A plot of lateral force, Fy, as a function of slip ratio and slip angle over the full range from -24 to 24 degrees is presented in Figure 9 for the bias belted tire. The maximum peak lateral force was developed at ±24 degrees of slip angle, which indicates that force saturation had not been attained. This maximum occurred at a slip ratio of -0.2, at large slip angles, and at 0 slip ratio when the slip angle was 0 degrees.

Selected plots for the bias belted, radial and bias tires are shown in Figures 10, 11, and 12, respectively. These represent slip angles of 0, ±4 and ±16 degrees. The lateral force characteristics of the radial and bias tires were very similar, whereas the bias belted tire seemed to develop slightly higher lateral forces during the application of traction.

Classical friction ellipses of the tire traction field are shown in Figure 13 for the entire slip angle range for the bias belted tire. Similar plots are included in Figures 14, 15 and 16 for the bias belted, radial and bias tires over the slip angle range of 0, ±4 and ±16 degrees. These plots show the relationship between lateral force and tractive force as a function of slip angle and contain the same force information as was presented in the previous plots. Although these plots lack slip ratio information, they are a valuable tool in analyzing tire traction behavior and can be readily described mathematically for modeling purposes. The well behaved nature of the tire and traction control system is exemplified by the shapes of the curves described by the locus of data points in these figures.

The aligning torque, Mz, was plotted against tractive force in Figures 17 through 20. A plot over the full range of slip angles for the bias belted tire is shown in Figure 17. The shape of this characteristic is rather complex and it is more meaningful to refer to the selected plots of Figures 18, 19 and 20 for the bias belted, radial and bias tires. When both the slip angle and aligning torque are positive, the torque is self aligning and tends to return the tire to zero steer. Application of traction tended to reverse this tendency in some cases which would result in a destabilization effect in steering behavior. At the condition where Fx=0 (no braking or driving) there was very little aligning torque at slip angles above ±16°. At smaller slip angles, however, the tires developed appreciable aligning torque, with the bias belted tire producing the greatest amount.

The influences of inclination angle, γ, and speed, V, on tire traction characteristics are shown in Figures 21 through 26. Figures 21, 22 and 23 show the braking traction behavior of the bias belted, radial and bias tires, respectively, at an inclination angle of 3 degrees. Similar characteristics are shown for these tires at an inclination angle of 6 degrees in Figures 24 through 26. Three speeds, 32, 64 and 96 km/h are represented in these plots. In all cases, traction decreased with increasing speed. There was negligible difference between 3 and 6 degree inclination angle traction data, indicating that the influence of camber angle is small.

Conclusion

The sample of tire test data, presented as a result of investigations that were conducted on the Calspan Tire Research Facility (TIRF), shows that much information can be obtained about tire traction behavior. This information permits understanding of wet tire traction characteristics and is presented in a form that can be used for computer simulation and analysis. Such studies can result in the prediction of vehicle behavior in wet driving situations where control of direction and speed is essential to safety.

Full "traction fields," relating tractive force and slip angle, can be quickly and repeatably developed under controlled conditions on TIRF. In addition, the effects of variations in inclination angle, slip ratio, load, road speed, inflation pressure, and water depth, as well as tire design, on traction characteristics can be determined through a laboratory simulation of desired tire operating conditions. All forces and moments that the tire produces in response to programmed inputs can be continuously monitored and recorded.

The presented results show the practicability of conducting wet-road traction testing on the TIRF laboratory facility to investigate and understand tire behavior.

References

1. Schuring, D.J. "Tire Parameter Determination" Volume II, December 1976, Report Number ZM-5563-T-2. Prepared for National Highway Traffic Safety Administration under Contract DOT-HS-00923.
2. Bird, K.D. and Martin, J.F., "The Calspan Tire Research Facility: Design, Development and Initial Test Results," presented at Automobile Engineering Meeting, Detroit, Michigan, May 14-18, 1973 SAE Paper 730582.
3. "Vehicle Dynamics Terminology SAE J670d," SAE Recommended Practice, published July 1975 by Society of Automotive Engineers, Inc.
4. Beauregard, C. F., "Peak Wet Braking Coefficient Measurement," Tire Science and Technology, TSTCA, Vol. 4, No. 1, Feb. 1976 pp 49-55.